10/31-96 JS ①

SANDIA REPORT

SAND96-8212 • UC-1409
Unlimited Release
Printed February 1996

Combustion of Porous Energetic Materials in the Merged-Flame Regime

Stephen B. Margolis, Forman A. Williams, Alexander M. Telengator

Prepared by
Sandia National Laboratories
Albuquerque, New Mexico 87185 and Livermore, California 94551
for the United States Department of Energy
under Contract DE-AC04-94AL85000

MASTER

SF2900Q(8-81)

BS

DISCLAIMER

Portions of this document may be illegible in electronic image products. Images are produced from the best available original document.

SAND96-8212 • UC-1409
Unlimited Release
Printed February 1996

COMBUSTION OF POROUS ENERGETIC MATERIALS IN THE MERGED-FLAME REGIME

STEPHEN B. MARGOLIS
Combustion Research Facility
Sandia National Laboratories
Livermore, California 94551 USA

and

FORMAN A. WILLIAMS and ALEXANDER M. TELENGATOR
Department of Applied Mechanics and Engineering Sciences
University of California, San Diego
La Jolla, California 92093 USA

Abstract

The structure and burning rate of an unconfined deflagration propagating through a porous energetic material is analyzed in the limit of merged condensed and gas-phase reaction zones. A global two-step reaction mechanism, applicable to certain types of degraded nitramine propellants and consisting of sequential condensed and gaseous steps, is postulated. Taking into account important effects due to multiphase flow and exploiting the limit of large activation energies, a theoretical analysis based on activation-energy asymptotics leads to explicit formulas for the deflagration velocity in a specifically identified regime that is consistent with the merged-flame assumption. The results clearly indicate the influences of two-phase flow and the multiphase, multi-step chemistry on the deflagration structure and the burning rate, and define conditions that support the intrusion of the primary gas flame into the two-phase condensed decomposition region at the propellant surface.

COMBUSTION OF POROUS ENERGETIC MATERIALS IN THE MERGED-FLAME REGIME

Introduction

There is increasing interest in the combustion behavior of systems characterized by significant two-phase flow. Examples include filtration combustion, smoldering, and the deflagration of porous energetic materials, where the latter, the focus of the present work, is of interest in propulsion and pyrotechnics. In such problems, the porous nature of the material arises from a certain degree of metastability which, after either a prolonged existence and/or exposure to an abnormal thermal environment, leaves the material in a chemically degraded, porous state. As a result, two-phase-flow effects associated with different velocities and properties of the condensed and gaseous species have a pronounced effect on the structure and propagation velocity of the combustion wave.

Although relatively complete formulations have been proposed for analyzing combustion phenomena involving multiphase flow [1], they are difficult to analyze because of the wide range of physical phenomena associated with such systems and the highly nonlinear nature of the problem. Accordingly, early two-phase work in this area tended to alleviate some of the difficulties by treating the two-phase medium as a single phase with suitably averaged properties [2,3]. Unfortunately, such models effectively require the velocity of each phase to be the same, precluding any analysis of two-phase-flow effects. More recently, however, it has proven possible to analyze deflagration models for porous energetic materials that explicitly involve multiphase flow [4–9]. These studies have largely been applicable to nitramine propellants, such as HMX and, in some cases, RDX, that are characterized by a liquid melt region in which extensive bubbling in an exothermic foam layer occurs. In some cases [4–6], two-phase-flow effects were confined to this layer, while in others [7–9], the solid material was assumed to be porous, with two-phase flow occurring throughout the preheat region. In order to focus on the effects of multiphase flow, chemistry was generally confined to a single-step overall reaction $R(c) \rightarrow P(g)$ representing direct conversion of condensed (melted) propellant to gaseous products. A generalization [5] in which a separate (primary) gas flame follows the initial multiphase decomposition region is given by $R(c) \rightarrow P(g)$, $R(c) \leftrightarrow R(g)$, $R(g) \rightarrow P(g)$, where $R(g)$ is a gaseous reactant. This scheme was applied to a nonporous problem to determine the structure and propagation velocity of a steady, planar nitramine deflagration, while stability results for these models have thus far been confined to single-step mechanisms [6,8,9].

The present work analyzes the limiting case in which the primary gas flame intrudes upon the multiphase decomposition region, a tendency that is often observed experimentally as the pressure increases. Thus, the single-step analysis [7] is extended by incorporating both condensed- and gas-phase reactions in the thin multiphase reaction region. In particular, a global sequential reaction mechanism is assumed, consisting of an overall condensed-phase reaction that produces gas-phase intermediates, and a gas-phase reaction that converts these intermediates to final products. While this mechanism is still an extreme approximation to actual nitramine chemistry [10,11], it enables us to fully incorporate two-phase flow into the analysis, and to assess its effect on the structure and propagation speed of the deflagration. The merged-flame analysis presented here is thus a multiphase-flow analog to single-phase studies of propagating combustion waves that are also governed by sequential reactions occurring in a single thin reaction zone [12–15].

The Mathematical Model

We consider an unconfined, steady, planar deflagration, propagating from right to left into a degraded (porous) energetic solid. Melting of the solid occurs at a moving location $\tilde{x} = \tilde{x}_m(\tilde{t})$ where the solid temperature equals its melting point $\tilde{T}_m$. Subsequent to melting, gas-phase intermediates are assumed to be produced directly by liquid-phase reactions, and these, in turn, react to form final combustion products according to the mechanism $R(c) \rightarrow I(g)$, $I(g) \rightarrow P(g)$, where $R(c)$, $I(g)$ and $P(g)$ denote the condensed (melted) reactant material, the intermediate gas-phase species, and the final gas-phase products. The pores within the solid are assumed to be filled with a mixture of $I(g)$ and $P(g)$, with the mass-fraction ratio ϕ of the two specified far upstream. The present analysis considers a merged regime in which both reactions occur within a single reaction zone, and thus, the deflagration wave consists of a solid/gas preheat region, the melting surface, a liquid/gas preheat region, a thin reaction zone in which all reactive species are converted to gaseous products, and the burned region. The latter typically corresponds to a dark zone that separates the primary flame from a secondary gas flame that has little effect on the burning rate.

A model describing a multiphase deflagration was derived previously for a single-step reaction mechanism $R(c) \rightarrow P(g)$ [7]. For two gas-phase species (I and P), an additional species conservation equation is thus required. For simplicity, we consider the single-temperature limit in which the rates of interphase heat transfer are large so that all phases have the same local temperature, but since a complete derivation of the full two-temperature model is given elsewhere [7,16], we provide only a brief explanation of the origin of each equation. Thus, we introduce, in terms of dimensional quantities (denoted by tildes) defined in the nomenclature, the nondimensional variables $x = \tilde{\rho}_s\tilde{c}_s\tilde{U}\tilde{x}/\tilde{\lambda}_s$, $t = \tilde{\rho}_s\tilde{c}_s\tilde{U}^2\tilde{t}/\tilde{\lambda}_s$, $T_{s,l,g} = \tilde{T}_{s,l,g}/\tilde{T}_u$, $u_{l,g} = \tilde{u}_{l,g}/\tilde{U}$, and $\rho_g = \tilde{\rho}_g/\tilde{\rho}_g^u$, where $\tilde{U} = -d\tilde{x}_m/d\tilde{t}$ is the (unknown) propagation speed of the melting front, and constant heat capacities and thermal conductivities have been assumed. We also define the parameters

$$r = \tilde{\rho}_l/\tilde{\rho}_s\,,\ \hat{r} = \tilde{\rho}_g^u/\tilde{\rho}_s\,,\ \ l = \tilde{\lambda}_l/\tilde{\lambda}_s\,,\ \ \hat{l} = \tilde{\lambda}_g/\tilde{\lambda}_s\,,\ \ b = \tilde{c}_l/\tilde{c}_s\,,\ \ \hat{b} = \tilde{c}_g/\tilde{c}_s\,,\ \ \gamma_s = \tilde{\gamma}_s/\tilde{c}_s\tilde{T}_u\,,$$
$$w = \tilde{W}_I/\tilde{W}_P\,,\ \ Le = \tilde{\lambda}_g/\tilde{\rho}_g\tilde{D}\tilde{c}_g\,,\ \ Q_{l,g} = \tilde{Q}_{l,g}/\tilde{c}_s\tilde{T}_u\,,\ \ N_{l,g} = \tilde{E}_{l,g}/\tilde{R}^\circ\tilde{T}_b\,, \tag{1}$$

$$\Lambda_l = \tilde{\lambda}_s\tilde{A}_l e^{-N_l}/\tilde{\rho}_s\tilde{c}_s\tilde{U}^2\,,\quad \Lambda_g = \tilde{\lambda}_s\tilde{A}_g(\tilde{\rho}_g^u)^n e^{-N_g}/\tilde{\rho}_s^2\tilde{c}_s\tilde{U}^2\,, \tag{2}$$

where n is the reaction order of the gas-phase reaction and Le is the gas-phase Lewis number. Here, $\tilde{\lambda}_g$, $\tilde{\rho}_g\tilde{D}$ and hence Le are assumed constant, r and $\hat{r}$ are density ratios (liquid-to-solid and upstream gas-to-solid), l and $\hat{l}$ are thermal conductivity ratios, b and $\hat{b}$ are heat-capacity ratios, w is the ratio of molecular weights of the two gas-phase species, γ_s is a heat-of-melting parameter (negative when melting is endothermic), $Q_{l,g}$ are heat-release parameters associated with the condensed and gas-phase reactions, $N_{l,g}$ are the activation energies, and $\Lambda_{l,g}$ are rate coefficients, or Damköhler numbers. Since $\Lambda_g/\Lambda_l = \hat{r}(\tilde{A}_g/\tilde{A}_s)(\tilde{\rho}_g^u)^{n-1}e^{N_l-N_g}$, we may regard Λ_l as the burning-rate eigenvalue.

For a steadily propagating deflagration, it is convenient to transform to the moving coordinate $\xi = x + t$ whose origin is defined to be $x_m(t)$. In the solid/gas region, the volume fraction α of gas is assumed constant ($\alpha = \alpha_s$), the solid phase is assumed to have constant density and zero velocity with respect to the laboratory frame of reference, and gas-phase continuity is given by

$$\frac{d}{d\xi}\left[\rho_g(u_g+1)\right] = 0\,,\quad \frac{d}{d\xi}\left[\hat{r}\rho_g Y(u_g+1)\right] = \left(\hat{l}/\hat{b}Le\right)\frac{d^2Y}{d\xi^2}\,,\quad \xi < 0\,, \tag{3}$$

representing overall continuity for the gas phase and mass conservation for the mass fraction Y of the gas-phase intermediates. In the liquid/gas region $\xi > 0$, overall continuity, continuity of the liquid phase, and continuity of the intermediate gas-phase species are given as

$$\frac{d}{d\xi}\left[r(1-\alpha)(u_l+1) + \hat{r}\alpha\rho_g(u_g+1)\right] = 0\,, \tag{4}$$

$$\left(d/d\xi\right)\left[(1-\alpha)(u_l+1)\right] = -\Lambda_l(1-\alpha)\,e^{N_l(1-T_b/T_l)}\,, \tag{5}$$

$$\frac{d}{d\xi}\left[\hat{r}\alpha\rho_g Y(u_g+1) + r(1-\alpha)(u_l+1)\right] = \left(\hat{l}/\hat{b}Le\right)\frac{d}{d\xi}\left[\alpha\frac{dY}{d\xi}\right] - \Lambda_g(\alpha\rho_g Y)^n\,e^{N_g(1-T_b/T_g)}, \tag{6}$$

where Eq. (5) has been used to eliminate the condensed-phase reaction-rate term that would have otherwise appeared in Eq. (6). Finally, overall energy conservation is given by

$$(1-\alpha_s)\frac{dT}{d\xi} + \hat{r}\hat{b}\alpha_s\frac{d}{d\xi}\left[\rho_g(u_g+1)T\right] = \frac{d}{d\xi}\left[(1-\alpha_s+\hat{l}\alpha_s)\frac{dT}{d\xi}\right],\quad \xi < 0\,, \tag{7}$$

$$\begin{aligned}\frac{d}{d\xi}\Big[r(1-\alpha)(u_l+1)(Q_l+Q_g+bT) + \hat{r}\alpha\rho_g(u_g+1)(Q_gY+\hat{b}T)\Big]&\\ = \frac{d}{d\xi}\Big\{\left[l(1-\alpha)+\hat{l}\alpha\right]\frac{dT}{d\xi} + (Q_g\hat{l}/\hat{b}Le)\alpha\frac{dY}{d\xi}\Big\},\quad \xi > 0\,,&\end{aligned} \tag{8}$$

where Eqs. (5) and (6) have been used to eliminate the reaction-rate terms in the latter.

The above system of equations is closed by adding an equation of state (assumed to be that of an ideal gas) and an expression for the liquid velocity u_l. An approximate analysis of gas-phase momentum conservation implies, for an unconfined, small Mach-number deflagration, that pressure is constant, thereby allowing the former to be expressed as $\rho_g T\,[Y + w(1-Y)] = \phi + w(1-\phi) \equiv \overline{\phi}$, where ϕ is defined below. An analysis of condensed-phase momentum and the assumption of zero velocity for the solid phase, on the other hand, leads to the kinematic approximation $u_l = (1-r)/r$ in the limit of small viscous and surface-tension-gradient forces [4,7]. The problem is then completely defined by imposing the boundary conditions $\alpha = \alpha_s$ for $\xi \le 0$, $u_g \to 0$, $Y \to \phi$ $(0 \le \phi \le 1)$, $T \to 1$ as $\xi \to -\infty$ and $\alpha \to 1$, $Y \to 0$. $T \to T_b$ as $\xi \to +\infty$, and the melting-surface conditions, which are continuity of $T = T_m$, u_g, Y and $dY/d\xi$ at $\xi = 0$ and the jump condition

$$[l(1-\alpha_s) + \hat{l}\alpha_s]\frac{dT}{d\xi}\bigg|_{\xi=0+} - (1-\alpha_s+\hat{l}\alpha_s)\frac{dT}{d\xi}\bigg|_{\xi=0-} = (1-\alpha_s)\,[-\gamma_s + (b-1)T_m]\,. \tag{9}$$

Here, the final burned temperature T_b is to be determined, as is the burning-rate eigenvalue Λ_l, which determines the propagation velocity of the deflagration according to Eq. (2).

Expressions for T_b and the burned gas velocity $u_g^b \equiv u_g\big|_{\xi=\infty}$, are obtained from the above model as follows. From Eqs. (3), (4) and the boundary conditions, we have the first integrals

$$\rho_g(u_g+1) = 1\,, \quad Y - \phi = \big(\hat{l}/\hat{r}\hat{b}Le\big)\frac{dY}{d\xi}\,, \quad \xi < 0\,, \tag{10}$$

$$(1-\alpha) + \hat{r}\alpha\rho_g(u_g+1) = \hat{r}\rho_g^b(u_g^b+1)\,, \quad \xi > 0\,, \tag{11}$$

where $\rho_g^b = \overline{\phi}/wT_b$ is the burned gas density. Thus, evaluating Eq. (11) at $\xi = 0$ using the first of Eqs. (10) and continuity across the melting surface, we obtain

$$u_g^b = \big[1 + \alpha_s(\hat{r}-1)\big]/\hat{r}\rho_g^b - 1 = \big[1+\alpha_s(\hat{r}-1)\big]wT_b/\hat{r}\overline{\phi} - 1\,. \tag{12}$$

Using these results, first integrals of the overall energy equations (7) and (8) are given by

$$(1-\alpha_s+\hat{r}\hat{b}\alpha_s)(T-1) = (1-\alpha_s+\hat{l}\alpha_s)\frac{dT}{d\xi}\,, \quad \xi < 0 \tag{13}$$

$$\begin{aligned}\big[b(1-\alpha) + \hat{b}(\alpha-\alpha_s+\alpha_s\hat{r})\big]T + (\alpha-\alpha_s+\alpha_s\hat{r})Q_gY &= \big[l(1-\alpha)+\hat{l}\alpha\big]\frac{dT}{d\xi} \\ + \big(Q_g\hat{l}/\hat{b}Le\big)\alpha\frac{dY}{d\xi} - (1-\alpha)(Q_l+Q_g) &+ \hat{b}(1-\alpha_s+\alpha_s\hat{r})T_b\,, \quad \xi > 0\,,\end{aligned} \tag{14}$$

Thus, subtracting Eq. (13) evaluated at $\xi = 0^-$ from Eq. (14) evaluated at $\xi = 0^+$ and using the melting-surface condition (9), we obtain

$$T_b = \big[(1-\alpha_s)(Q_l+Q_g+1+\gamma_s) + \hat{r}\alpha_s(\phi Q_g + \hat{b})\big]\Big/\hat{b}\big[1+\alpha_s(\hat{r}-1)\big]\,. \tag{15}$$

This result, which can be derived from a more general two-temperature model [16], is independent of the particular form of the gas-phase equation of state. In the limit $Q_g \to 0$, Eq. (15) collapses to the result obtained for the single-step model [7]. Equations (10), (13) and (14), being first integrals of Eqs. (3), (7) and (8), now take the place of the latter in our model.

Equations (12) and (15) imply that there are significant variations in T_b and u_g^b with the upstream gas-to-solid density ratio $\hat{r}$, which in turn is proportional to the pressure $\tilde{p}_g^\circ$ according to $\hat{r} \equiv \tilde{\rho}_g^u/\tilde{\rho}_s = \tilde{W}_I\tilde{p}_g^\circ/\tilde{\rho}_s\tilde{R}^\circ\tilde{T}_u\overline{\phi}$. This important effect arises from the thermal expansion of the gas, the two-phase nature of the flow in the solid/gas and liquid/gas regions, and the fact that, for nonzero α_s, some of the heat released by combustion must be used to help raise the temperature of the gas-phase species within the porous solid from unity to T_b [7]. Consequently, both T_b and u_g^b are typically decreasing functions of $\hat{r}$. An additional effect, revealed by the two-step reaction analysis, is that T_b does not depend just on the total heat release $Q_l + Q_g \equiv Q$ associated with the complete conversion of the energetic solid to final gas products, but also on the heat release Q_g specifically associated with the gas-phase reaction. This, too, is a two-phase-flow effect that arises from the fact that reactive intermediate species exist within the voids in the porous solid, and the heat released by these intermediates affects the final burned temperature, which, for a given total heat release Q, increases as the fractional heat release associated with the gas-phase reaction increases.

The Asymptotic Limit and the Outer Solution

Further analytical development leading to the determination of Λ_l requires an analysis of the reactive liquid/gas region $\xi > 0$. Equations (5), (6) and (14) constitute three equations for Y, T and α in this region, with u_g then determined from Eq. (11) and the equation of state, and the eigenvalue Λ_l determined by the boundary conditions. In order to handle the Arrhenius nonlinearities in Eqs. (5) and (6), we exploit the largeness of the activation energies $N_{g,l}$ and consider the formal asymptotic limit $N_{g,l} \gg 1$ such that $N_g/N_l = \nu \sim \mathrm{O}(1)$ and $\beta \equiv (1-T_b^{-1})N_l \gg 1$, where β is the Zel'dovich number. This ordering of the activation energies, along with a corresponding order relation for the ratio Λ_g/Λ_l to be introduced shortly, helps to insure that both the condensed and gas-phase reactions are active in a single thin reaction zone, since departures from these orderings can result in separated reaction zones [17].

In the limit $\beta \to \infty$, the Arrhenius terms are exponentially small unless T is within $\mathrm{O}(1/\beta)$ of T_b. Consequently, all chemical activity is concentrated in a zone whose thickness is $\mathrm{O}(1/\beta)$. On the scale of the (outer) coordinate ξ, this thin region is a sheet whose location is denoted by $\xi_r = x_r - x_m$, where $x_r > x_m$. Hence, the liquid/gas region is comprised of a preheat zone

$(0 < \xi < \xi_r)$ where chemical activity is exponentially small, the thin reaction zone where the two chemical reactions are active and go to completion, and a burned region $\xi > \xi_r$. Denoting the outer solutions on either side of the reaction zone by a zero superscript, we conclude from Eq. (5), (10) – (12) and the equation of state,

$$\alpha_0^0 = \begin{cases} \alpha_s\,, & \xi < \xi_r \\ 1\,, & \xi > \xi_r \end{cases}, \quad u_g + 1 = [(\alpha - \alpha_s + \hat{r}\alpha_s)/\hat{r}\alpha\overline{\phi}]\,[Y + w(1 - Y)]T\,, \tag{16}$$

where the latter is valid for all ξ. Thus, there is a jump in α^0, and hence in u_g^0, across the reaction zone. Similarly, in obtaining the complete outer solution for Y and T, it is necessary to connect the solutions on either side of the reaction zone by deriving appropriate jump conditions across $\xi = \xi_r$. This will entail an analysis of the inner reaction-zone structure, whereupon an asymptotic matching of the inner and outer solutions will yield these jump conditions and an expression for Λ_l. In connection with this procedure, it is convenient, and physically appealing, to attempt a representation of the reaction-rate terms in Eqs. (5) and (6) as delta-function distributions with respect to the outer spatial variable ξ [12,13]. Using the results (16), the system of equations for the outer variables Y^0 and T^0 thus become

$$\hat{r}(Y^0 - \phi) = (\hat{l}/\hat{b}Le)\frac{dY^0}{d\xi}\,, \quad \xi < 0\,; \qquad (1/r)\frac{d\alpha^0}{d\xi} = P_l\delta(\xi - \xi_r)\,, \quad \xi > 0\,, \tag{17}$$

$$\frac{d}{d\xi}\left[(\alpha^0 - \alpha_s + \hat{r}\alpha_s)Y^0 - \alpha^0\right] = (\hat{l}/\hat{b}Le)\frac{d}{d\xi}\left(\alpha^0\frac{dY^0}{d\xi}\right) - P_g\delta(\xi - \xi_r - H)\,, \quad \xi > 0\,, \tag{18}$$

$$\left(1 - \alpha_s + \hat{r}\hat{b}\alpha_s\right)\left(T^0 - 1\right) = \left(1 - \alpha_s + \hat{l}\alpha_s\right)\frac{dT^0}{d\xi}\,, \quad \xi < 0\,, \tag{19}$$

$$\begin{aligned}\left[b(1 - \alpha^0) + \hat{b}(\alpha^0 - \alpha_s + \alpha_s\hat{r})\right]T^0 + (\alpha^0 - \alpha_s + \alpha_s\hat{r})Q_gY^0 &= \left[l(1 - \alpha^0) + \hat{l}\alpha^0\right]\frac{dT^0}{d\xi} \\ + (Q_g\hat{l}/\hat{b}Le)\alpha^0\frac{dY^0}{d\xi} - (1 - \alpha^0)(Q_l + Q_g) &+ \hat{b}(1 - \alpha_s + \alpha_s\hat{r})T_b\,, \quad \xi > 0\,,\end{aligned} \tag{20}$$

where P_l and P_g are the source strengths of the distributions at $\xi = \xi_r$ and $\xi = \xi_r + H$. Here, P_l, P_g and H are to be determined, where the $O(1/\beta)$ width of the merged reaction zone implies that H is of this order (or smaller) as well.

The solution of Eqs. (17) - (20) subject to the melting and boundary conditions is given by $P_l = (1 - \alpha_s)/r$, $P_g = 1 - \alpha_s + \hat{r}\alpha_s\phi$,

$$Y^0(\xi) = \begin{cases} \phi + \left[(1-\phi)(1-\alpha_s) - (1-\alpha_s+\hat{r}\alpha_s\phi)e^{-(1-\alpha_s+\hat{r}\alpha_s)\hat{b}LeH/\hat{l}}\right]e^{\hat{r}\hat{b}Le(\xi-\xi_r)/\hat{l}}/(1-\alpha_s+\hat{r}\alpha_s), & \xi < \xi_r \\ \left[(1-\alpha_s+\hat{r}\alpha_s\phi)/(1-\alpha_s+\hat{r}\alpha_s)\right]\left[1 - e^{(1-\alpha_s+\hat{r}\alpha_s)\hat{b}Le(\xi-\xi_r-H)/\hat{l}}\right], & \xi_r < \xi < \xi_r + H \\ 0, & \xi > \xi_r + H\,, \end{cases} \tag{21}$$

$$T^0(\xi) = \begin{cases} 1 + (T_m - 1)\,e^{[(1-\alpha_s+\hat{r}\hat{b}\alpha_s)/(1-\alpha_s+\hat{l}\alpha_s)]\xi}, & \xi < 0 \\ B + (T_m - B)\,e^{\{[b(1-\alpha_s)+\hat{r}\hat{b}\alpha_s]/[l(1-\alpha_s)+\hat{l}\alpha_s]\}\xi}, & 0 < \xi < \xi_r \\ B_1 + (T_b - B_1)\,e^{\hat{b}(1-\alpha_s+\hat{r}\alpha_s)(\xi-\xi_r-H)/\hat{l}}, & \xi_r < \xi < \xi_r + H \\ T_b = B_1 + (1-\alpha_s+\hat{r}\alpha_s\phi)Q_g/\hat{b}(1-\alpha_s+\hat{r}\alpha_s), & \xi > \xi_r + H\,, \end{cases} \tag{22}$$

where

$$B=[(1-\alpha_s)(1+\gamma_s)+\hat{r}\hat{b}\alpha_s]/[b(1-\alpha_s)+\hat{r}\hat{b}\alpha_s],\quad B_1=[(1-\alpha_s)(Q_l+1+\gamma_s)+\hat{r}\hat{b}\alpha_s]/\hat{b}(1-\alpha_s+\hat{r}\alpha_s)$$

$$\xi_r=\{[l(1-\alpha_s)+\hat{l}\alpha_s]/[b(1-\alpha_s)+\hat{r}\hat{b}\alpha_s]\}\ln\{[B_1-B+(T_b-B_1)e^{-\hat{b}(1-\alpha_s+\hat{r}\alpha_s)H/\hat{l}}]/(T_m-B)\}. \quad (23)$$

A sketch of the outer solution is shown in Fig. 1. Since the interval $\xi_r < \xi < H$ lies within the merged reaction zone, only that portion of Eqs. (21) and (22) for $\xi < \xi_r$ and $\xi > \xi_r + H$ actually represents the outer solution. Consequently, there is an O(H) jump in Y^0 and T^0 across this zone [from $\xi = \xi_r^-$ to $\xi = (\xi_r + H)^+$]. Alternatively, for small H, an expansion of $\delta(\xi - \xi_r - H)$ in Eq. (18) about $H = 0$ introduces the derivative $\delta'(\xi - \xi_r)$ [13], which implies discontinuities in Y^0 and T^0 at $\xi = \xi_r$. These discontinuities are determined by H, which, like Λ_l, is an eigenvalue. Both are calculated by matching the outer solution to that of the inner reaction-zone problem.

Reaction-Zone Solutions

To analyze the chemical boundary layer at ξ_r, we introduce a stretched inner variable $\eta = \beta(\xi - \xi_r)$ and a normalized temperature $\Theta = (T-1)/(T_b-1)$. We then seek solutions in this region as $\alpha \sim \alpha_0 + \beta^{-1}\alpha_1 + \cdots$, $u_g \sim u_0 + \beta^{-1}u_1 + \cdots$, $Y \sim \beta^{-1}y_1 + \beta^{-2}y_2 + \cdots$, $\Theta \sim 1 + \beta^{-1}\theta_1 + \cdots$, $\Lambda_l \sim \beta(\Lambda_0 + \beta^{-1}\Lambda_1 + \cdots)$ and $H \sim \beta^{-1}h_1 + \beta^{-2}h_2 + \cdots$, where the u_i are calculated in terms of the α_i, y_i and θ_i from Eq. (16), which is valid in the reaction zone. We also order the rate-coefficient ratio $\Lambda_g/\Lambda_l = \hat{r}(\tilde{\rho}_g^u)^{n-1}(\tilde{A}_g/\tilde{A}_l)\, e^{(1-\nu)N_l} \equiv \beta^n\lambda$, where λ is an O(1) parameter. This scaling, along with the previous ordering of the activation energies, partly defines one regime that is consistent with a merged reaction-zone structure.

Substituting these expansions into Eqs. (5), (6) and (14), the leading-order inner variables α_0, y_1 and θ_1 are governed by

$$\frac{d\alpha_0}{d\eta} = r\Lambda_0(1-\alpha_0)\, e^{\theta_1}\,, \quad (24)$$

$$[l + (\hat{l} - l)\alpha_0]\frac{d\theta_1}{d\eta} + [\hat{l}Q_g/\hat{b}Le(T_b-1)]\alpha_0\frac{dy_1}{d\eta} = \{[(b-\hat{b})T_b + Q_l + Q_g]/(T_b-1)\}(1-\alpha_0)\,, \quad (25)$$

$$(\hat{l}/\hat{b}Le)\frac{d}{d\eta}\Big(\alpha_0\frac{dy_1}{d\eta}\Big) = -\frac{d\alpha_0}{d\eta} + \lambda\Lambda_0\big(\alpha_0 y_1\overline{\phi}/wT_b\big)^n e^{\nu\theta_1}\,. \quad (26)$$

Solutions to these equations as $\eta \to \pm\infty$ must match with the outer solution as $\xi \uparrow \xi_r^-$ and as $\xi \downarrow (\xi_r + H)^+$, leading to the matching conditions

$$\alpha_0 \to 1\,,\quad \theta_1 \to 0\,,\quad y_1 \to 0 \ \text{ as } \eta \to +\infty\,, \quad (27)$$

$$\alpha_0 \to \alpha_s\,,\quad \theta_1 \sim E_1\eta + E_2h_1\,,\quad y_1 \sim (\hat{b}Le/\hat{l})\,[-\hat{r}\eta + (1-\alpha_s+\hat{r}\alpha_s\phi)h_1] \ \text{ as } \eta \to -\infty\,,$$
$$E_1 = [(T_b-B)/(T_b-1)]\frac{b(1-\alpha_s)+\hat{r}\hat{b}\alpha_s}{l(1-\alpha_s)+\hat{l}\alpha_s},\quad E_2 = -[(T_b-B_1)/(T_b-1)]\frac{\hat{b}}{\hat{l}}(1-\alpha_s+\hat{r}\alpha_s). \quad (28)$$

Solution of the complete inner problem given by Eqs. (27) - (31) will only be possible for certain values of h_1 and Λ_0, the leading-order coefficients in the expansions of H and Λ_l.

Employing α_0 as the independent variable, Eqs. (25) and (26) take the form

$$\left[l+(\hat{l}-l)\alpha_0\right]e^{\theta_1}\frac{d\theta_1}{d\alpha_0}+\left[\hat{l}Q_g/\hat{b}Le(T_b-1)\right]\alpha_0 e^{\theta_1}\frac{dy_1}{d\alpha_0}=\left[(b-\hat{b})T_b+Q_l+Q_g\right]/(T_b-1)r\Lambda_0\,, \quad (29)$$

$$\left(r\Lambda_0\hat{l}/\hat{b}Le\right)\frac{d}{d\alpha_0}\left[\alpha_0(1-\alpha_0)e^{\theta_1}\frac{dy_1}{d\alpha_0}\right]=-1+(\lambda/r)\left(\alpha_0 y_1\overline{\phi}/wT_b\right)^n e^{(\nu-1)\theta_1}/(1-\alpha_0)\,. \quad (30)$$

A closed-form solution to this system is not readily apparent, and thus further analytical development is restricted to a perturbation analysis of Eqs. (29) and (30) in the limit that Q_g is small relative to Q_l. Since this implies that most of the heat release occurs in the first stage of the two-step reaction process, at least some of the initial exothermic gas-phase decomposition reactions should be lumped with the overall reaction (1a), regarding the resulting decomposition products as the gas-phase intermediates $I(g)$. Thus, we formally introduce a small bookkeeping parameter ϵ, where $O(\beta^{-1})\ll\epsilon\ll O(1)$, and write $Q_g=\epsilon Q_g^1$, where $Q_g^1\sim O(1)$. We now seek solutions to the leading-order inner problem in the form $\alpha_0\sim\alpha_0^0+\epsilon\alpha_0^1+\cdots$, $y_1\sim y_1^0+\epsilon y_1^1+\cdots$, $\theta_1\sim\theta_1^0+\epsilon\theta_1^1+\cdots$, $\Lambda_0\sim\Lambda_0^0+\epsilon\Lambda_0^1+\cdots$, and $h_1\sim h_1^0+\epsilon h_1^1+\cdots$.

Substituting these latest expansions into Eqs. (24), (29) and (30), a closed subsystem

$$\left[l+(\hat{l}-l)\alpha_0^0\right]e^{\theta_1^0}\frac{d\theta_1^0}{d\alpha_0^0}=\left[(b-\hat{b})B_1+Q_l\right]/(B_1-1)r\Lambda_0^0\,,\qquad \frac{d\alpha_0^0}{d\eta}=r\Lambda_0^0(1-\alpha_0^0)\,e^{\theta_1^0} \quad (31)$$

is obtained, subject to $\alpha_0^0\to 1$, $\theta_1^0\to 0$ as $\eta\to+\infty$, and $\alpha_0^0\to\alpha_s$, $\theta_1^0\sim E_1^0\eta$ as $\eta\to-\infty$, where E_1^0 is given by E_1 in Eq. (28) with T_b replaced by its leading-order approximation B_1. The first of Eqs. (31) is readily integrated from $\alpha_0^0=\alpha_s$ (at $\eta=-\infty$) to any $\alpha_0^0\le 1$ ($\eta\le+\infty$) to give

$$e^{\theta_1^0(\alpha_0^0)}=\left[(b-\hat{b})B_1/(B_1-1)r\Lambda_0^0\right]\int_{\alpha_s}^{\alpha_0^0}d\overline{\alpha}/\left[l+(\hat{l}-l)\overline{\alpha}\right]. \quad (32)$$

Evaluating Eq. (32) at $\alpha_0^0=1$ (at which $\theta_1^0=0$) thus determines Λ_0^0 as

$$\Lambda_0^0=\begin{cases}\left\{[(b-\hat{b})B_1+Q_l]/(B_1-1)r(\hat{l}-l)\right\}\ln\left\{\hat{l}/[l+(\hat{l}-l)\alpha_s]\right\}, & l\neq\hat{l}\\ (1-\alpha_s)[(b-\hat{b})B_1+Q_l]/(B_1-1)rl, & l=\hat{l}.\end{cases} \quad (33)$$

Substituting this result into Eq. (32) for arbitrary α_0, we thus obtain

$$\theta_1^0(\alpha_0^0)=\begin{cases}\ln\left\{\ln[l+(\hat{l}-l)\alpha_0^0]-\ln[l+(\hat{l}-l)\alpha_s]\right\}-\ln\left\{\ln\hat{l}-\ln[l+(\hat{l}-l)\alpha_s]\right\}, & \hat{l}\neq l\\ \ln(\alpha_0^0-\alpha_s)-\ln(1-\alpha_s), & \hat{l}=l.\end{cases} \quad (34)$$

The determination of $\alpha_0^0(\eta)$, and hence $\theta_1^0(\eta)$, then follows directly from the second of Eqs. (35). For example, when $\hat{l}=l$ (equal gas and liquid thermal conductivities), we obtain

$$\alpha_0^0(\eta)=\left\{\alpha_s+e^{[(b-\hat{b})B_1+Q_l](1-\alpha_s)\eta/l(B_1-1)}\right\}\Big/\left\{1+e^{[(b-\hat{b})B_1+Q_l](1-\alpha_s)\eta/l(B_1-1)}\right\}, \quad (35)$$

where the matching condition at $\eta = -\infty$ has been used to evaluate the constant of integration.

From Eq. (33), the leading-order expression for Λ_l is independent of the effects of the second reaction, which has been assumed to have a relatively small thermal effect. Consequently, the first effects of the two-step mechanism on the burning rate appear at $O(\epsilon)$, which requires the calculation of Λ_0^1. We proceed by first calculating y_1^0, which is determined from the leading-order version of Eq. (30). For simplicity, we consider the parameter regime $\alpha_s = \alpha_s^1 \epsilon$, $\hat{l} = l + \epsilon \hat{l}^1$ and $\nu = 1 + \epsilon \nu^1$, corresponding to $O(\epsilon)$ porosities, $O(\epsilon)$ differences in the conductivities of the condensed and gaseous phases, and $O(\epsilon\beta)$ differences in the activation energies of the two reaction steps. Also, we consider only a first-order gas-phase reaction ($n = 1$), and assume that $(\lambda\overline{\phi}/rw\Lambda_0^0 T_b^0)(\hat{b}Le/rl) = \lambda_0 + \epsilon\lambda_1$, where $T_b^0 = (Q_l + 1 + \gamma_s)/\hat{b}$ is the leading-order approximation to T_b with respect to ϵ. The parameter group $(\lambda\overline{\phi}/rw\Lambda_0^0 T_b^0)(\hat{b}Le/rl)$ is a gas-to-liquid ratio of diffusion-weighted reaction rates, referred to as consumption rates [12,13], which represent relative rates of depletion, taking into account both chemical reaction and, for the gas phase, species diffusion. The fact that larger Lewis numbers are associated with higher rates of depletion of the gaseous reactant stems from the higher concentration of this species in the reaction zone that results from a smaller mass diffusivity.

In the parameter regime just outlined, θ_1^0 and Λ_0^0 simplify to

$$\theta_1^0 = \ln \alpha_0^0, \quad \Lambda_0^0 = \left[bQ_l + (b - \hat{b})(1 + \gamma_s)\right]/rl(Q_l + 1 + \gamma_s - \hat{b}), \quad \alpha_0^0(\eta) = e^{r\Lambda_0^0 \eta}/\left[1 + e^{r\Lambda_0^0 \eta}\right], \tag{36}$$

or $\eta = (1/r\Lambda_0^0)\ln[\alpha_0^0/(1 - \alpha_0^0)]$. Hence, the leading-order version of Eq. (30) for y_1^0 is given by

$$\frac{d^2 y_1^0}{d{\alpha_0^0}^2} + \left(\frac{2}{\alpha_0^0} - \frac{1}{1 - \alpha_0^0}\right)\frac{dy_1^0}{d\alpha_0^0} - \frac{\lambda_0 y_1^0}{\alpha_0^0(1 - \alpha_0^0)^2} = -\frac{(\hat{b}Le/rl\Lambda_0^0)}{(\alpha_0^0)^2(1 - \alpha_0^0)}, \tag{37}$$

subject to $y_1^0 \to 0$ as $\alpha_0^0 \to 1$. An appropriate matching condition as $\alpha_0^0 \to 0$, however, cannot be obtained directly from Eq. (28) because that equation was derived under the assumption that $\alpha_s \neq 0$, whereas to leading order in ϵ, α_s is zero. Indeed, at this level of approximation, the outer variable Y^0 has no meaning for $\xi < 0$, since there is essentially no gas in this region. To derive proper matching conditions on y_1^0 and, for later use, y_1^1, we consider the local mass fraction Z of the intermediate gas-phase species with respect to the total mass of all species, gaseous and condensed [16]. Thus, $Z = \hat{r}\alpha\rho_g Y/[\hat{r}\alpha/\rho_g + r(1-\alpha)] = \hat{r}\overline{\phi}\alpha Y/\{\hat{r}\overline{\phi}\alpha + r(1-\alpha)[Y + w(1-Y)]T\}$ is unambiguous as $\alpha \to 0$, where it must vanish. From the outer solution written in terms of η, the required behavior of Z as $\eta \to -\infty$ is $Z \sim \epsilon\beta^{-1}(\hat{r}\overline{\phi}\alpha_s^1 \hat{b}Le/rwT_b^0 l)(-\hat{r}\phi\eta + h_1^0)$. Hence, substituting the inner expansions into the definition of Z and imposing this asymptotic behavior implies

$$\alpha_0^0 y_1^0 \to 0\,, \quad \alpha_0^0 y_1^1 \sim -\alpha_s^1 y_1^0 + \alpha_s^1(\hat{b}Le/l)\left[-(\hat{r}\phi/r\Lambda_0^0)\ln\alpha_0^0 + h_1^0\right] \text{ as } \alpha_0^0 \to 0\,, \tag{38}$$

where we have written these conditions in terms of α_0^0, using the fact that $\alpha_0^1 \to \alpha_s^1$ as $\alpha_0^0 \to 0$.

Formal solutions to Eq. (37) can be expressed in terms of hypergeometric functions, but since we desire explicit representations for use in the next-order problem, we focus on such solutions that may be obtained for certain values of λ_0. In particular, solutions for $\lambda_0 = 1$ [16] and $\lambda_0 = 4$ that satisfy the matching conditions are given by

$$y_1^0 = -(\hat{b}Le/2rl\Lambda_0^0) \cdot \begin{cases} 1 + \left[(1-\alpha_0^0)/\alpha_0^0\right] \ln\left[(1-\alpha_0^0)/\alpha_0^0\right] + \ln \alpha_0^0/\alpha_0^0(1-\alpha_0^0), & \lambda_0 = 1 \\ (3-\alpha_0^0)/(1-\alpha_0^0) + 2\ln \alpha_0^0/(1-\alpha_0^0)^2, & \lambda_0 = 4\,. \end{cases} \tag{39}$$

We observe that although $\alpha_0^0 y_1^0 \to 0$ as $\alpha_0^0 \to 0$, y_1^0 itself is unbounded, exhibiting the behavior

$$y_1^0 \sim -(\hat{b}Le/rl\Lambda_0^0) \cdot \begin{cases} \ln \alpha_0^0, & \lambda_0 = 1 \\ \ln \alpha_0^0 + 3/2, & \lambda_0 = 4 \end{cases} \qquad \text{as } \alpha_0^0 \to 0\,. \tag{40}$$

Profiles of the leading-order inner variables as functions of η are shown in Fig. 2.

The reaction-zone problem at the next order in ϵ determines α_0^1, y_1^1, θ_1^1 and Λ_0^1, as well as h_1^0, which is still unknown. As before, the problem for α_0^1 and θ_1^1 decouples and is given by

$$\frac{d\alpha_0^1}{d\eta} = r\left[\Lambda_0^0(1-\alpha_0^0)\theta_1^1 + \Lambda_0^1(1-\alpha_0^0) - \Lambda_0^0\alpha_0^1\right]e^{\theta_1^0}\,, \tag{41}$$

$$l\frac{d\theta_1^1}{d\eta} + \hat{l}^1\alpha_0^0\frac{d\theta_1^0}{d\eta} + \left[lQ_g^1/\hat{b}Le(T_b^0-1)\right]\alpha_0^0\frac{dy_1^0}{d\eta} = -C_0\alpha_0^1 + C_1(1-\alpha_0^0)\,, \tag{42}$$

$$\alpha_0^1 \to 0\,,\ \theta_1^1 \to 0 \ \text{ as } \eta \to +\infty; \quad \alpha_0^1 \to \alpha_s^1\,,\ \theta_1^1 \sim E_1^1\eta + E_2^1 h_1^0 \ \text{ as } \eta \to -\infty\,, \tag{43}$$

where

$$\begin{gathered} C_0 = \left[(b-\hat{b})T_b^0 + Q_l\right]/(T_b^0-1) = rl\Lambda_0^0\,, \quad C_1 = \left[Q_g^1(T_b^0-1) + T_b^1(Q_l+\hat{b}-b)\right]/(T_b^0-1)^2\,, \\ E_1^1 = \alpha_s^1(\hat{r}\hat{b}-b)/l + \left[\alpha_s^1(T_b^0-1) + T_b^1\right](1+\gamma_s-b)/l(T_b^0-1)^2\,, \quad E_2^1 = -Q_g^1/l(T_b^0-1)\,, \end{gathered} \tag{44}$$

and $T_b \sim T_b^0 + \epsilon T_b^1 + \cdots$, with $T_b^0 = (Q_l + 1 + \gamma_s)/\hat{b}$ and $T_b^1 = Q_g^1/\hat{b} - \hat{r}(T_b^0-1)\alpha_s^1$. We observe that T_b^1, and hence C_1 and E_1^1, all depend on α_s^1, reflecting, to this order of approximation, a linearly decreasing dependence of the burned temperature on the porosity of the solid.

Transforming to α_0^0 as the independent variable, Eqs. (41) and (42) become

$$\frac{d\alpha_0^1}{d\alpha_0^0} + \frac{\alpha_0^1}{1-\alpha_0^0} = \theta_1^1 + \Lambda_0^1/\Lambda_0^0\,, \tag{45}$$

$$rl\Lambda_0^0\alpha_0^0\frac{d\theta_1^1}{d\alpha_0^0} + C_0\frac{\alpha_0^1}{(1-\alpha_0^0)} = C_1 - r\hat{l}^1\Lambda_0^0\alpha_0^0 - \left\{Q_g^1 rl\Lambda_0^0/[\hat{b}Le(T_b^0-1)]\right\}(\alpha_0^0)^2\frac{dy_1^0}{d\alpha_0^0}\,, \tag{46}$$

subject to Eq. (43) expressed in terms of α_0^0. Rewriting Eq. (45) as $(d/d\alpha_0^0)[\alpha_0^1/(1-\alpha_0^0)] = (\theta_1^1 + \Lambda_0^1/\Lambda_0^0)/(1-\alpha_0^0)$ and substituting this result into the derivative of Eq. (46), we obtain

$$\frac{d^2\theta_1^1}{d\alpha_0^{0\,2}} + \frac{1}{\alpha_0^0}\frac{d\theta_1^1}{d\alpha_0^0} + \frac{\theta_1^1}{\alpha_0^0(1-\alpha_0^0)} = -\frac{Q_g^1}{\hat{b}\,Le(T_b^0-1)}\frac{1}{\alpha_0^0}\frac{d}{d\alpha_0^0}\left[(\alpha_0^0)^2\frac{dy_1^0}{d\alpha_0^0}\right] - \frac{\Lambda_0^1/\Lambda_0^0}{\alpha_0^0(1-\alpha_0^0)} - \frac{\hat{l}^1/l}{\alpha_0^0}\,, \tag{47}$$

where y_1^0 is given by Eq. (39). Homogeneous solutions of Eq. (47) are $(1-\alpha_0^0)\ln\left[\alpha_0^0(1-\alpha_0^0)^{-1}\right]+1$ and $1-\alpha_0^0$, so that the general solution for θ_1^1 may be constructed by reduction of order and substituted into Eq. (45) to determine α_0^1. Thus, for example,

$$\begin{aligned}\theta_1^1 &= c_1\left[1+(1-\alpha_0^0)\ln\left(\frac{\alpha_0^0}{1-\alpha_0^0}\right)\right]+c_2(1-\alpha_0^0)-\frac{\Lambda_0^1}{\Lambda_0^0}+\frac{\hat{l}^1}{2l}(1-\alpha_0^0)\ln\alpha_0^0\\ &+\frac{Q_g^1}{rl\Lambda_0^0(T_b^0-1)}\left\{\frac{11-9\alpha_0^0}{2(1-\alpha_0^0)}+\frac{\ln\alpha_0^0}{(1-\alpha_0^0)^2}-\frac{5\ln\alpha_0^0}{2(1-\alpha_0^0)}-2\ln\alpha_0^0+\frac{13}{2}(1-\alpha_0^0)\ln\left(\frac{\alpha_0^0}{1-\alpha_0^0}\right)\right.\\ &\left.+2(1-\alpha_0^0)\left[\frac{\pi^2}{6}+\mathrm{Li}_2(\alpha_0^0)\right]\ln\alpha_0^0+2\mathrm{Li}_2(1-\alpha_0^0)-2(1-\alpha_0^0)\left[2\mathrm{Li}_3(\alpha_0^0)+\mathrm{Li}_3(1-\alpha_0^0)\right]\right\},\end{aligned}\tag{48}$$

$$\begin{aligned}\alpha_0^1 &= c_3(1-\alpha_0^0)+(1-\alpha_0^0)\left[c_1\alpha_0^0\ln\left(\frac{\alpha_0^0}{1-\alpha_0^0}\right)+c_2\alpha_0^0+\frac{\hat{l}^1}{2l}\left(\alpha_0^0\ln\alpha_0^0-\alpha_0^0\right)\right]\\ &+\frac{Q_g^1(1-\alpha_0^0)}{rl\Lambda_0^0(T_b^0-1)}\left\{\frac{1}{2(1-\alpha_0^0)}\left(1+\frac{\ln\alpha_0^0}{1-\alpha_0^0}\right)-\left[\frac{1+4\alpha_0^0}{2(1-\alpha_0^0)}-\left(\frac{\pi^2}{3}+\frac{13}{2}\right)\alpha_0^0\right]\ln\alpha_0^0\right.\\ &\left.-\frac{13}{2}\alpha_0^0\ln(1-\alpha_0^0)+2\alpha_0^0\mathrm{Li}_2(\alpha_0^0)\ln\alpha_0^0-2\mathrm{Li}_2(1-\alpha_0^0)-4\alpha_0^0\mathrm{Li}_3(\alpha_0^0)-2\alpha_0^0\mathrm{Li}_3(1-\alpha_0^0)\right\},\end{aligned}\tag{49}$$

for $\lambda_0=4$, where c_1, c_2 and c_3 are integration constants, and the polylogarithms $\mathrm{Li}_n(\alpha)$, $n\geq 2$, are defined recursively for all complex α by $\mathrm{Li}_2(\alpha)=-\int_0^\alpha \hat{\alpha}^{-1}\ln(1-\hat{\alpha})\,d\hat{\alpha}=\sum_{j=1}^\infty \alpha^j/j^2$, $\mathrm{Li}_{n>2}(\alpha)=\int_0^\alpha \hat{\alpha}^{-1}\mathrm{Li}_{n-1}(\hat{\alpha})\,d\hat{\alpha}=\sum_{j=1}^\infty \alpha^j/j^n$, where the series representation is convergent for $|\alpha|\leq 1$ [18]. For $0\leq\alpha\leq 1$, $\mathrm{Li}_2(\alpha)$ and $\mathrm{Li}_3(\alpha)$ are monotonic functions that range from $\mathrm{Li}_2(0)=\mathrm{Li}_3(0)=0$ to $\mathrm{Li}_2(1)=\pi^2/6$ and $\mathrm{Li}_3(1)\doteq 1.20205690$. Also, $\mathrm{Li}_2(\alpha)+\mathrm{Li}_2(1-\alpha)=\pi^2/6-\ln\alpha\,\ln(1-\alpha)$, which was used to obtain Eqs. (48) and (49). Application of the matching conditions then determines Λ_0^1, c_1, $c_2(h_1^0)$ and c_3 as

$$\begin{aligned}&\Lambda_0^1=Q_g^1(21-2\pi^2)/6rl(T_b^0-1)+E_1^1/r-\Lambda_0^0\hat{l}^1/2l,\ c_2=Q_g^1\{[3-\pi^2+6\mathrm{Li}_3(1)]/3r\Lambda_0^0-h_1^0\}/l(T_b^0-1),\\ &c_1=-Q_g^1(9+\pi^2)/3rl\Lambda_0^0(T_b^0-1)+E_1^1/r\Lambda_0^0-\hat{l}^1/2l,\ c_3=\alpha_s^1+Q_g^1(2\pi^2-3)/6rl\Lambda_0^0(T_b^0-1).\end{aligned}\tag{50}$$

An expression for h_1^0 may be determined by continuing with the perturbation analysis, but it can be deduced directly from the second matching condition (38) which, for $\lambda_0=4$, gives

$$y_1^1\sim\alpha_s^1(\hat{b}Le/\Lambda_0^0)\left[(1-\hat{r}\phi)\ln\alpha_0^0+r\Lambda_0^0h_1^0+3/2\right]/\alpha_0^0\quad\text{as}\quad\alpha_0^0\to 0\,.\tag{51}$$

Since $1/\alpha_0^0\sim\exp(-r\Lambda_0^0\eta)$ as $\eta\to-\infty$, Eq. (51) implies that y_1^1 grows exponentially as $\eta\to-\infty$ unless the right-hand side is identically zero. Since only algebraic growth of the inner solution is compatible with an asymptotic matching with the outer solution, as indicated in Eq. (28), we conclude from Eq. (51) that $\hat{r}\phi=1+\mathrm{O}(\epsilon)$ and $h_1^0=(-3/2)/(r\Lambda_0^0)$. This required restriction of $\hat{r}$ to values that are relatively close to $1/\phi\geq 1$ corresponds to high upstream gas-phase densities, or pressures, and may be interpreted as a compatibility condition, required for the existence of a merged-flame solution, that accompanies our ordering of the activation energies and consumption rates when gas-phase heat release is small. According to Eq. (16) for u_g, it essentially limits the two-phase-flow effect to that associated with thermal expansion of the gas. Larger rates of gas-phase transport relative to the condensed phase would cause the gas-phase reaction to occur increasingly downstream of the condensed reaction, leading to a breakdown in the merged-flame structure analyzed here, but it is anticipated that larger gas-phase consumption rates would allow for larger gas-phase convective transport arising from smaller upstream gas densities. Profiles of α_0^1 and θ_1^1 for $\lambda_0 = 4$ are shown in Fig. 2.

Discussion of the Burning Rate and Conclusions

The dimensional propagation speed $\tilde{U}$, from the definition of Λ_l given in Eq. (2), is given by

$$\begin{aligned}\tilde{U}^2 &\sim (\tilde{\lambda}_s \tilde{A}_l/\tilde{\rho}_s \tilde{c}_s)\beta^0\left[1+\epsilon T_b^1(2-T_b^0)/T_b^0(T_b^0-1)+\cdots\right](\Lambda_0^0+\epsilon\Lambda_0^1+\cdots)^{-1}e^{-N_l^0(1-\epsilon T_b^1/T_b^0+\cdots)} \\ &\sim (\tilde{\lambda}_s \tilde{A}_l/\tilde{\rho}_s \tilde{c}_s)(\beta^0/\Lambda_0^0)e^{-N_l^0}e^{\epsilon\beta^0 T_b^1/(T_b^0-1)+\cdots}\left\{1+\epsilon[T_b^1(2-T_b^0)/T_b^0(T_b^0-1)-\Lambda_0^1/\Lambda_0^0]+\cdots\right\},\end{aligned} \tag{52}$$

where T_b, which appears in the definitions of the nondimensional activation energy N_l and the Zel'dovich number β, has been expanded according to the expansion given below Eq. (44), and we have introduced the ϵ-independent definitions $N_l^0 \equiv \tilde{E}_l/\tilde{R}^\circ\tilde{T}_b^0$ and $\beta^0 \equiv (T_b^0-1)N_l^0/T_b^0$. Substituting the expressions obtained in the previous section for Λ_0^0 and Λ_0^1 and setting the bookkeeping parameter ϵ equal to unity (implying $\alpha_s^1 \equiv \alpha_s$, $\hat{l}^1 \equiv \hat{l} - l$ and $Q_g^1 = Q_g$), we obtain the asymptotic expression for the burning rate, in the specific merged-flame parameter regime considered here, as

$$\begin{aligned}\tilde{U}^2 \sim\ & (\tilde{\lambda}_s \tilde{A}_l/\tilde{\rho}_s \tilde{c}_s)\left[rl(T_b^0-1)/(bT_b^0-1-\gamma_s)\right]\beta^0 e^{-N_l^0}e^{\beta^0[Q_g/\hat{b}(T_b^0-1)-\alpha_s/\phi]+\cdots}\Big\{1+(\hat{l}-l)/2l \\ & +\left[Q_g/(T_b^0-1)(bT_b^0-1-\gamma_s)\right]\left[(2-T_b^0)(bT_b^0-1-\gamma_s)/\hat{b}T_b^0-(21-2\pi^2)/6-(1+\gamma_s-b)/\hat{b}\right] \\ & -\left[\alpha_s/(bT_b^0-1-\gamma_s)\phi\right]\left[(2-T_b^0)(bT_b^0-1-\gamma_s)/T_b^0+(T_b^0-1)(\hat{b}-\phi b)-(1-\phi)(1+\gamma_s-b)\right]+\cdots\Big\}\end{aligned} \tag{53}$$

for $\lambda_0 = 4$, with a similar expression for $\lambda_0 = 1$. The first effects of heat release associated with the second step of the reaction model are determined by the terms proportional to Q_g in Eq. (53).

The dominant effects associated with gas-phase heat release are determined by the second exponential factor in Eq. (53), which is exponentially large unless $\alpha_s/Q_g \approx \hat{b}^{-1}(T_b^0-1)^{-1}\phi$. Values of α_s/Q_g less (greater) than this critical value thus produce a significant increase (decrease) in the burning rate over that of a nonporous material governed solely by the condensed reaction, corresponding to whether or not the perturbation in the burned temperature, which arises from nonzero porosity and the additional heat release associated with the gas-phase reaction, is positive or negative. Since Q_g is positive, the additional heat release associated with the gas-phase reaction enhances the burning rate, but decreasing amounts of solid material that correspond to increasing porosities lead to a lower overall heat release associated with the condensed-phase reaction, resulting in a critical value of porosity for which these counteracting effects balance. Plots of $U = \tilde{U}(Q_g, \alpha_s)/\tilde{U}(0,0)$ are shown in Fig. 3.

Although the primary effect associated with nonzero porosity and a second gas-phase reaction step is thus thermodynamic in nature, additional effects are revealed by those terms arising from the correction Λ_0^1 to the leading-order burning-rate eigenvalue Λ_0^0, which give rise to the last two terms proportional to both Q_g and α_s and the term proportional to $\hat{l} - l$ within the curly brackets in Eq. (53). For example, it is readily seen that a value of the gas-phase thermal conductivity greater (less) than that of the liquid phase tends to increase (decrease) the propagation speed, since larger values of $\hat{l} - l$ allow for greater heat transport from the reaction zone back to the preheat region, providing a type of "excess enthalpy" effect for the condensed phase portion of the reaction. The result for the case in which $\lambda_0 = 1$, corresponding to a smaller pre-exponential reaction-rate coefficient for the gas-phase reaction, is identical to Eq. (53), except for the fact that the numerator $21 - 2\pi^2 \doteq 1.26$ is replaced by $\pi^2 - 6 \doteq 3.87$ in the second term proportional to Q_g in that equation. Thus, as expected, a smaller gas-phase consumption rate results in a smaller overall burning rate when the corresponding rate for the condensed-phase reaction is unchanged.

In conclusion, the present analysis has sought to describe some of the effects associated with the deflagration of porous energetic materials arising from two-phase-flow in the presence of a multiphase sequential reaction mechanism. In contrast to previous work in which the condensed and gas-phase reactions were spatially separated, a merged-flame parameter regime, in which both reactions are operative and proceed to completion in a single thin reaction zone, was considered in the present study. Although additional parameter constraints were required to support a merged-flame structure, such a structure was calculated for the case of a high-pressure deflagration in which the relative flow of gas with respect to the condensed material arises primarily from thermal expansion of the former. This result is consistent with typical experiments involving the nitramine propellants HMX and RDX that show the tendency of the primary gas flame to move closer to the propellant surface as the pressure increases. Further parametric studies are in progress and will be reported in future publications.

Nomenclature

$\tilde{A}$	pre-exponential rate coefficient
$\tilde{D}$	mass diffusion coefficient
$\tilde{c}$	heat capacity
$\tilde{E}$	activation energy
$\tilde{Q}$	heat release
$\tilde{R}^{\circ}$	gas constant
$\tilde{t}$	time
$\tilde{T}$, Θ, θ	temperature variable
$\tilde{u}$	velocity variable
$\tilde{U}$	propagation speed
$\tilde{W}$	molecular weight
$\tilde{x}$, ξ, η	spatial coordinate
Y, y	gas-phase mass-fraction variable
α	gas-phase volume fraction
$\tilde{\gamma}_s$	heat of melting
$\tilde{\lambda}$	thermal conductivity
$\tilde{\rho}$	density
ϕ	gas-phase mass-fraction ratio

Subscripts, superscripts:

g, l, s	gas, liquid, solid phase
b	downstream burned value
m	melting-surface value
u	upstream unburned value

Acknowledgements

This work was supported by the U. S. Department of Energy under Contract DE-AC04-94AL85000 and by a Memorandum of Understanding between the Office of Munitions (Department of Defense) and the Department of Energy. AMT was supported by a President of Russia Scholarship for Study Abroad.

References

1. Baer, M. R., and Nunziato, J. W., *Int. J. Multiphase Flow* 12:861–889 (1986).
2. Maksimov, E. I., and Merzhanov, A. G., *Combust. Explos. Sh. Waves* 2:25–31 (1966).
3. Merzhanov, A. G., *Combust. Flame* 13:143–156 (1969).
4. Margolis, S. B., Williams, F. A., and Armstrong, R. C., *Combust. Flame* 67:249–258 (1987).
5. Li, S. C., Williams, F. A., and Margolis, S. B., *Combust. Flame* 80:329–349 (1990).
6. Margolis, S. B., and Williams, F. A., *Combust. Flame* 79:199–213 (1990).
7. Margolis, S. B., and Williams, F. A., *J. Propulsion Power* 11:759–768 (1995a).
8. Margolis, S. B., and Williams, F. A., *Combust. Sci. Technol.* 106:41–68 (1995b).
9. Margolis, S. B., and Williams, F. A., *Int. J. Multiphase Flow*, in press (1996).
10. Prasad, K., Yetter, R. A., and Smooke, M. D., Yale University Report ME-101-95, 1995.
11. Li, S. C., and Williams, F. A., *J. Propulsion and Power*, in press (1996).
12. Margolis, S. B., and Matkowsky, B. J., *SIAM J. Appl. Math.* 42:1175–1188 (1982a).
13. Margolis, S. B., and Matkowsky, B. J., *Combust. Sci. Technol.* 27:193–213 (1982b).
14. Peláez, J., and Liñán, A., *SIAM J. Appl. Math.* 45:503–522 (1985).
15. Booty, M. L., Holt, J. B., and Matkowsky, B. J., *Q. Jl. Mech. Appl. Math.* 43:224–249 (1990).
16. Margolis, S. B., *Int. J. Eng. Math.*, submitted (1996).
17. Peláez, J., *SIAM J. Appl. Math.* 47:781–799 (1987).

FIGURE CAPTIONS

Fig. 1. Outer structure of the leftward-propagating deflagration wave. The solid/gas region lies to the left of $\xi = 0$, and the liquid/gas region to the right. The shaded area denotes the region $\xi_r < \xi < \xi_r + H$, which, despite the explicit representation afforded by the outer delta-function formulation, actually lies within the inner reaction zone. The region to the right of the reaction zone consists of purely gaseous products. Parameter values used were $b = r = Le = l = \phi = 1$, $\hat{b} = \hat{r} = \hat{l} = .8$, $\alpha_s = .25$, $Q_l = 5$, $Q_g = H = .5$, $\gamma_s = -.2$, $T_m = 2$.

Fig. 2. Inner structure of the leftward-propagating deflagration wave for the case $\lambda_0 = 4$. The curves were drawn for the parameter regime analyzed in the paper, based on the parameter values used in Fig. 1 (choosing $\epsilon = .5$, the latter imply that the scaled parameters $\alpha_s^1 = \alpha_s/\epsilon = .5$, $Q_g^1 = Q_g/\epsilon = 1$ and $\hat{l}^1 = (\hat{l} - l)/\epsilon = -.4$).

Fig. 3. Approximate nondimensional propagation speed $U = \tilde{U}(Q_g, \alpha_s)/\tilde{U}(0,0)$, corresponding to the case $\lambda_0 = 4$, as a function of α_s for $Q_g = .1$ (solid), .2 (dash), .3 (chain-dash), .4 (dot) and .5 (chain-dot), where the remaining parameter values were taken to be the same as those used in the previous figures.

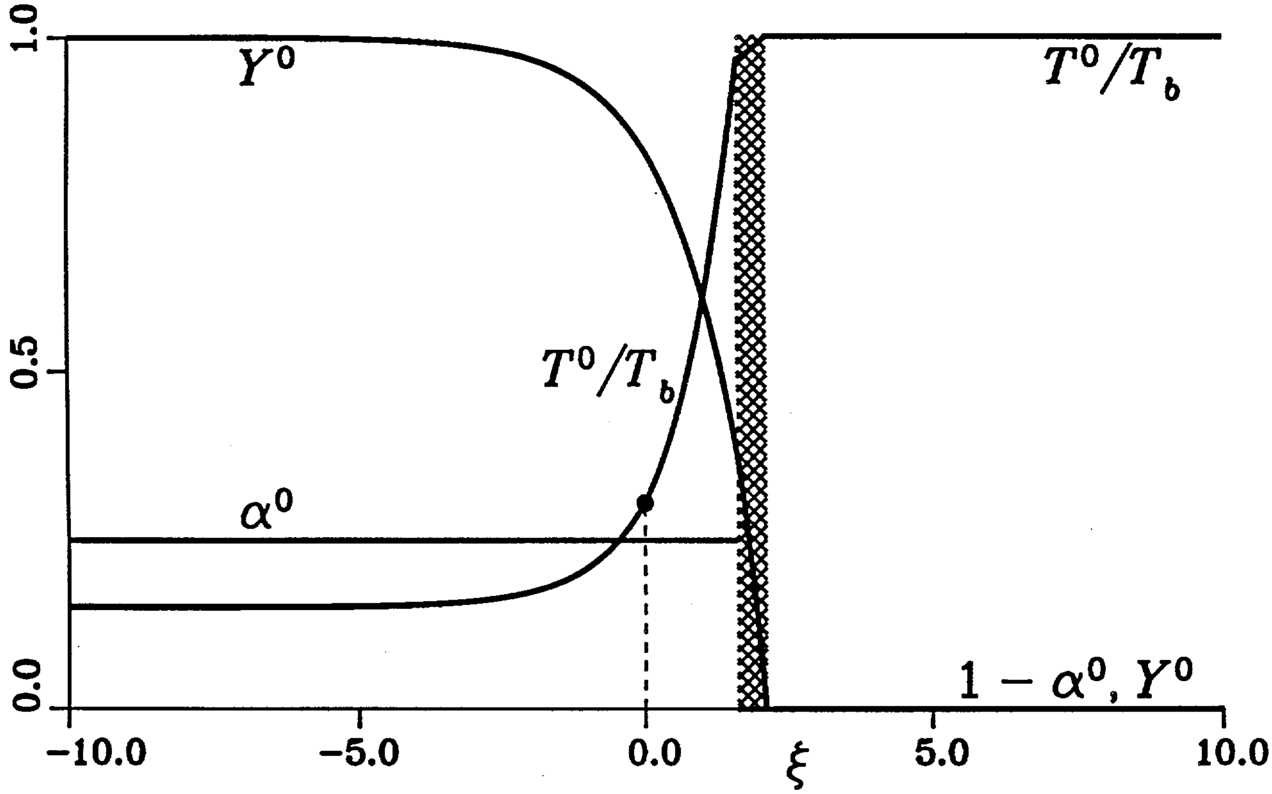

Figure 1

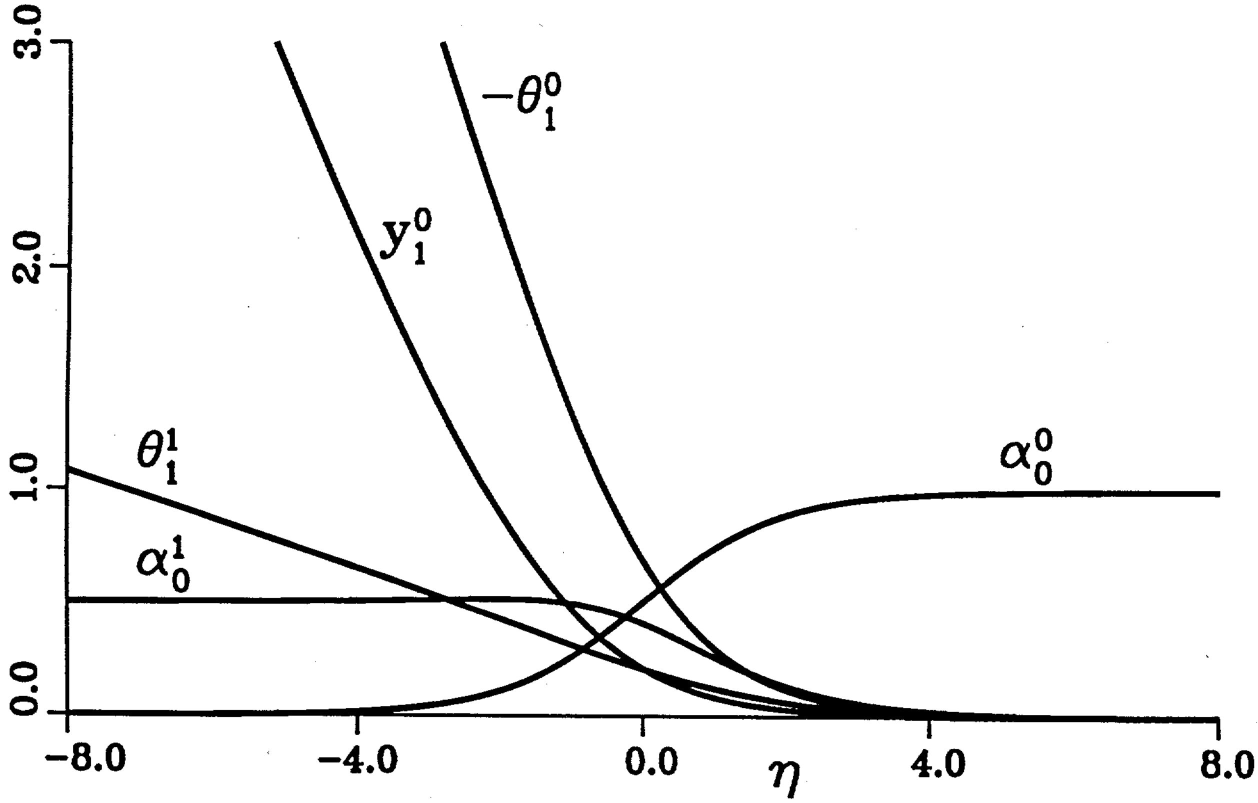
3.0
2.0
1.0
0.0
$-\theta_1^0$
y_1^0
θ_1^1
α_0^1
α_0^0
−8.0
−4.0
0.0
η
4.0
8.0

Figure 2

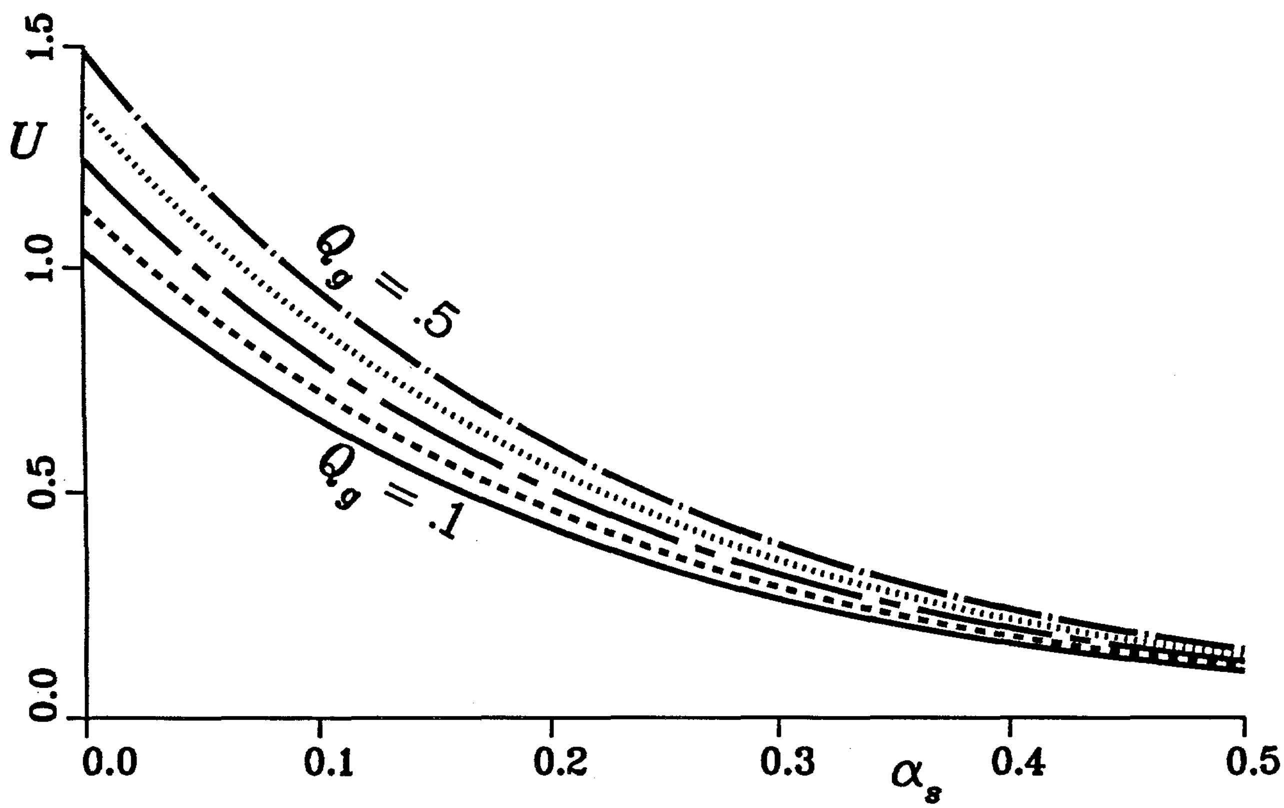

Figure 3

UNLIMITED RELEASE

INITIAL DISTRIBUTION

Dr. John K. Bechtold
Department of Mathematics
New Jersey Institute of Technology
Newark, NJ 07102-1982

Dr. Mitat A. Birkan
Program Manager
Directorate of Aerospace and Engineering Sciences
Department of the Air Force
Bolling Air Force Base, DC 20332-6448

Prof. Michael Booty
Department of Mathematics
New Jersey Institute of Technology
Newark, NJ 07102-1982

Prof. John D. Buckmaster
Department of Aeronautical and Astronautical Engineering
University of Illinois
Urbana, IL 61801

Prof. Sebastien Candel
Ecole Central des Arts et Manufactures
Grande Voie de Vignes
92290 Chatenay-Malabry
FRANCE

Dr. John Card
Department of Mechanical Engineering
Yale University
New Haven, CT 06520

Prof. J. F. Clarke
College of Aeronautics
Cranfield Institute of Technology
Cranfield-Bedford MK43 OAL
ENGLAND

Prof. Paul Clavin
Laboratoire Dynamique et Thermophysique des Fluides
Universite de Provence
Centre Saint Jerome
13397 Marseille Cedex 4
FRANCE

Prof. F. E. C. Culick
Jet Propulsion Center
California Institute of Technology
Pasadena, CA 91125

Prof. Martin Golubitsky
Department of Mathematics
University of Houston
University Park
Houston, TX 77004

Prof. Michael Gorman
Department of Physics
University of Houston
Houston, TX 77004

Dr. Daryl D. Holm
CNLS, MS 457
Los Alamos National Laboratory
Los Alamos, NM 87545

Prof. G. M. Homsy
Department of Chemical Engineering
Stanford University
Stanford, CA 94305

Dr. G. Joulin
Laboratoirie D'Energetique et de Detonique
Universite de Poitiers
Rue Guillaume VII
86034 Poitiers
FRANCE

Dr. Hans Kaper
Applied Mathematics Division
Argonne National Laboratory
9700 S. Cass Ave.
Argonne, IL 60439

Prof. A. K. Kapila
Department of Mathematical Sciences
Rensselaer Polytechnic Institute
Troy, NY 12128

Prof. D. R. Kassoy
Department of Mechanical Engineering
University of Colorado
Boulder, CO 80309

Prof. Joseph B. Keller
Department of Mathematics
Stanford University
Stanford, CA 94305

Prof. Barbara Keyfitz
Department of Mathematics
University of Houston
University Park
Houston, TX 77004

Prof. C. K. Law
Department of Mechanical and Aerospace Engineering
Engineering Quadrangle
Princeton University
Princeton, NJ 08544

Dr. Gary Leaf
Applied Mathematics Division
Argonne National Laboratory
9700 S. Cass Avenue
Argonne, IL 60439

Prof. Amable Liñán
Universidad Politecnica de Madrid
Escuela Tecnica Superior de Ingenieros Aeronauticos
Plaza del Cardenal Cisneros, 3
Madrid - 3
SPAIN

Prof. J. T. C. Liu
Division of Engineering, Box D
Brown University
Providence, RI 02912

Prof. Moshe Matalon
Department of Engineering Sciences and Applied Mathematics
Northwestern University
Evanston, IL 60208

Prof. Bernard J. Matkowsky
Department of Engineering Sciences and Applied Mathematics
Northwestern University
Evanston, IL 60208

Prof. A. C. McIntosh
Department of Fuel and Energy
University of Leeds
Leeds LS2 9JT
United Kingdom

Prof. D. O. Olagunju
Department of Mathematical Sciences
University of Delaware
Newark, DE 19716

Prof. R. E. O'Malley
Department of Applied Mathematics
University of Washington Seattle, WA 98195

Prof. Norbert Peters
Institute fur Allgemeine Mechanik
Technische Hochschule Aachen
Aachen
GERMANY

Prof. John Ross
Department of Chemistry
Stanford University
Stanford, CA 94305

Prof. Victor Roytburd
Department of Mathematical Sciences
Rensselaer Polytechnic Institute
Troy, NY 12128

Prof. W. A. Sirignano
Office of the Dean
School of Engineering
University of California, Irvine
Irvine, CA 92717

Prof. L. Sirovich
Division of Applied Mathematics, Box F
Brown University
Providence, RI 02912

Prof. G. I. Sivashinsky
Department of Mathematics
Tel-Aviv University
Ramat-Aviv, Tel-Aviv 69978
ISRAEL

Prof. Mitchell D. Smooke
Department of Mechanical Engineering
Yale University
New Haven, CT 06520

Prof. D. Scott Stewart
Department of Theoretical and Applied Mechanics
University of Illinois
Urbana, IL 61801

Prof. C. H. Su
Division of Applied Mathematics, Box F
Brown University
Providence, RI 02912

Prof. Cesar Treviño
Departmento de Termica y Fluidos
Universidad Nacional Autonoma de Mexico
Facultad de Ingenieria
Patios No. 12, Jardines del Sur
MEXICO 23, D.F.

Prof. Vladimir Volpert
Department of Engineering Sciences and Applied Mathematics
Northwestern University
Evanston, IL 60208

Dr. David Weaver
Air Force Rocket Propulsion Laboratory
DYP/Stop 24
Edwards Air Force Base, CA 93523

Prof. Forman A. Williams
Department of Applied Mechanics and Engineering Sciences
University of California, San Diego
La Jolla, CA 92093

Prof. Vigor Yang
Department of Mechanical Engineering
Pennsylvania State University
University Park, PA 16802

Prof. Benn Zinn
Department of Aerospace Engineering
Georgia Institute of Technology
225 North Avenue, NW
Atlanta, GA 30332

C. K. Westbrook, LLNL, L-321

MS 1110 R. C. Allen, 1422
MS 0834 A. C. Ratzel, 9112
MS 0834 M. R. Baer, 9112
MS 0834 M. L. Hobbs, 9112
MS 0834 R. J. Gross, 9112

MS 9001 T. O. Hunter, 8000
MS 9405 R. E. Stoltz, 8008
MS 9004 M. E. John, 8100
MS 9213 S. C. Johnston, 8103
MS 9054 W. J. McLean, 8300
MS 9163 W. Bauer, 8302
MS 9053 C. M. Hartwig, 8345
MS 9051 S. B. Margolis, 8351 (30)
MS 9051 L. A. Rahn, 8351
MS 9051 W. T. Ashurst, 8351
MS 9051 A. R. Kerstein, 8351
MS 9055 R. Behrens, 8353
MS 9056 G. A. Fisk, 8355
MS 9052 D. R. Hardesty, 8361
MS 9053 R. W. Carling, 8362
MS 9021 Technical Communications Department, 8815, for OSTI (10)
MS 9021 Technical Communications Department, 8815/Technical Library, MS 0899, 4414
MS 0899 Technical Library, 4414 (4)
MS 9018 Central Technical Files, 8950-2 (3)